Journal Name

RSCPublishing

ARTICLE

Metallic Cyanoacetylides of Copper, Silver and Gold: Generation and Structural Characterization

Carlos Cabezas,[a] Carmen Barrientos,[b] Antonio Largo,[b*] Jean-Claude Guillemin[c] and J. L. Alonso[a*]

The metallic cyanoacetylides CuCCCN, AgCCCN, and AuCCCN have been synthesized in the throat of a pulsed supersonic expansion by reaction of metal vapors, produced by laser ablation, and BrCCCN. Their pure rotational spectra in the $(X^1\Sigma^+)$ electronic ground state were observed by Fourier transform microwave spectroscopy in the 2-10 GHz frequency region. Importantly, the rotational spectroscopy constants determined from the analysis of the rotational spectra clearly established the existence of metal-CCCN arrangements for all the mentioned cyanoacetylides. A study of the chemical bonding by means of a topological analysis of the electron density helps to understand the preferences for metal-C bonding over the metal-N bonding.

Introduction

The study of metal cyanides provides a good field to explore the nature of the metal-carbon chemical bonding in organometallic species, as well as the competition between C-metal type and N-metal type isomers. Several experimental studies have been carried out to explore the detailed molecular structure of first-row transition metal cyanides/isocyanides.[1-10] Rotational spectroscopy studies[1-6] led to the observation of the cyanides for Cr, Co, Ni, Cu, and Zn. However, both cyanide and isocyanide isomers were observed for Fe being the cyanide isomer the most stable form.[8,9] Theoretical studies have also proved to be useful for rationalizing this MCN/MNC behavior of cyanides and isocyanides of first-row transition metals. Of particular relevance is the theoretical study by Frenking et al.[11] of cyanides and isocyanides of Cu, Ag and Au. These authors provided an analysis of the molecular structure, relative stability, and bonding analysis of MCN/MNC (M=Cu, Ag, Au). They found that the cyanide isomer is clearly preferred over the isocyanide one for Group 11 elements and provided a theoretical explanation for this preference. In agreement with most experimental observations, early transition metals were found to favor the isocyanide isomer, whereas late transition metals tend to prefer the cyanide arrangement.[12] With the exception of the FeCN/FeNC system, which is still a challenge for theoretical methods,[13] for the rest of first-row transition metals a reasonable agreement between theoretical predictions and experimental evidence is observed.

Up to date, only two longer metal cyanides C_nN chains have been studied. Endo and cowokers[14] reported the detection of two silicon-bearing carbon chain radicals, SiCCN and SiCCCN by Fourier transform microwave spectroscopy. The radicals were generated in a supersonic jet by a pulsed electric discharge of gas mixture of $SiCl_4$, CH_3CN or HC_3N. On the other hand, aluminum cyanoacetylide AlCCCN[15] was produced in our lab using laser ablation molecular beam Fourier transform microwave (LA-MB-FTMW) spectroscopy.[16] These three related systems, SiCCN, SiCCCN and AlCCCN, show as common structural feature the preference to the Metal-C arrangement, being in reasonable agreement with the theoretical predictions.

In the present work, we reported on the first experimental and theoretical study of cyanoacetylides for Group 11 elements the MC_3N (M= Cu, Ag and Au). They have been synthesized within the environment of a transient plasma by the reaction of metal vapours, produced by laser ablation of metallic rods in presence of BrCCCN, and characterized in a supersonic expansion by Fourier transform microwave spectroscopy. The experimental investigation is accompanied by a series of theoretical calculations having a dual goal in mind: aiding in the assignment of the rotational spectra by providing precise rotational parameters and analyzing the nature of the metallic bonding paying special attention to the competition between MCCCN and MNCCC isomers and to the electrostatic/covalent nature of the bond.

Methods

Experimental. Measurements on each of CuC_3N, AgC_3N and AuC_3N were conducted using a LA-MB-FTMW spectrometer[17] constructed at the University of Valladolid operating in the 2-10 GHz frequency range. It consists in a cylindrical stainless-steel high vacuum chamber, which contains a Fabry-Pérot resonator formed by two spherical aluminum mirrors of 70 cm of diameter and 70 cm of radius of curvature. In this investigation, the pulsed nozzle system has been modified by addition of a home-made heatable reservoir extension, placed to hold liquid and/or solid compounds which can be used as precursors of metal bearing species (Figure 1). This is accommodated in the backside of one of the mirrors, aligned
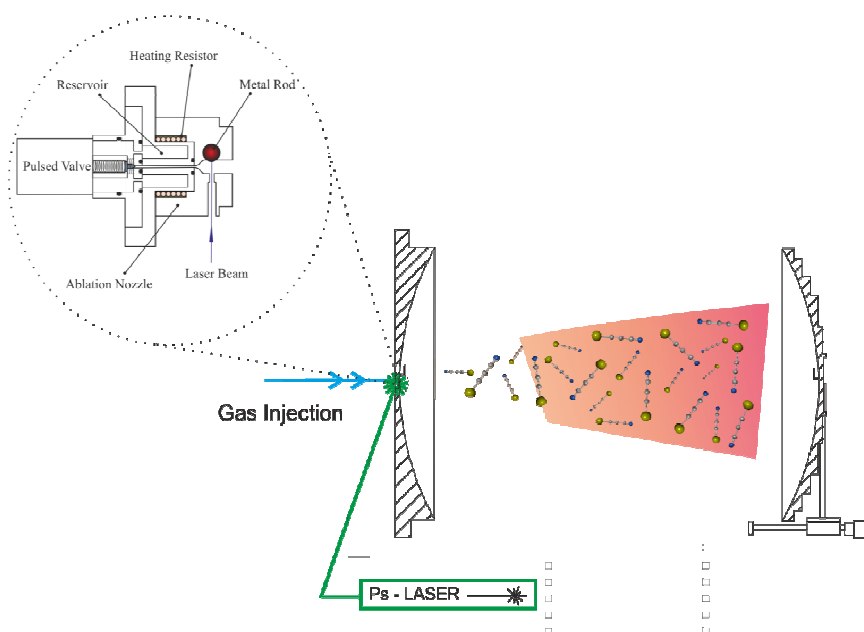
Figure 1. Configuration of the heating-reservoir with laser ablation capabilities developed for present studies (see text).

accommodated in the backside of one of the mirrors, aligned parallel relative to the optical axis of the resonator. Using this device, CuC_3N, AgC_3N and AuC_3N were created by laser ablation of pure metal rods in the throat of a pulsed supersonic expansion of Ne and BrCCCN (prepared as previously reported)[15] as described below.

Solid samples of BrCCCN placed in the heatable reservoir were vaporized at ca. 65 °C creating a mixture by flowing Ne (10 bars stagnation pressure) through the reservoir. This mixture was flowed over either the copper, silver or gold target rod which was ablated (after an adequate delay) using a picosecond Nd:YAG-laser pulse (λ = 355 nm and 10 mJ pulse^{-1}), vaporizing the solid and producing plasma which trigger the chemical reactions in the precursor mixture.[15,18,19] A motorized micrometer is used to simultaneously rotate and translate the sample rod each laser pulse, so the laser hits a different point of the sample surface in successive pulses, minimizing the problem of shot-to-shot fluctuation in the amount of the desorbed material. Immediately, the resulting products are supersonically expanded and rapidly cooled to a rotational temperature of ~2 K between the two mirrors of the Fabry–Pérot resonator. Then a microwave pulse ($0.3\mu s$) is applied, producing the macroscopic polarization of the species in the jet. Once the excitation ceases, molecular relaxation gives rise to a transient emission signal (free induction decay) at microwave frequencies, which is captured in the time domain. Its Fourier transformation to the frequency domain yields the rotational transitions that appear as Doppler doublets, because the supersonic jet travels parallel to the resonator axis (see Figure 1). The rest frequencies are calculated as the arithmetic mean of the Doppler doublets and are obtained with accuracy better than 3 kHz. Typically 100-200 pulses were accumulated to achieve an adequate signal-to-noise ratio.

Theoretical. Geometry optimizations of CuC_3N, AgC_3N, and AuC_3N species were carried out at the second-order Møller-Plesset (MP2) level of theory. For carbon, nitrogen, and copper atoms we employed the all-electron Dunning's correlated consistent triple-zeta ba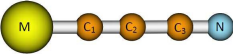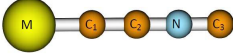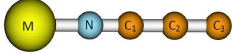sis sets augmented with diffuse and polarization functions, usually denoted as aug-cc-pVTZ.[20,21] For silver and gold atoms the aug-cc-pVTZ+PP basis set was used. This basis set includes a small-core relativistic pseudo-potential[22] (Ar+3d orbitals for Ag and Kr+4d3f orbitals for Au) combined with an aug-cc-pVTZ basis set[23] for outer electrons. In such a way 28 inner electrons for silver and 60 inner electrons for gold are treated through pseudo-potentials, thus making affordable the application of correlated methods. The reliability of the method of calculation has been tested in the case of copper cyanide. The MP2/aug-cc-pVTZ predicted equilibrium rotational constant for CuCN, namely 4229 MHz is not far from the experimentally measured[1] rotational constant of 4224.9768 MHz. Furthermore, the predicted bond distances in CuCN at that level of theory (1.8169 and 1.1776 Å for the Cu-C and C-N distances, respectively) are nearly within 0.01 Å of the experimental values.[1] Therefore, it seems that the MP2/aug-cc-pVTZ level of calculation could be reliable for predictive purposes in this type of compounds.

Harmonic vibrational calculations were carried out for the species obtained through geometry optimizations in order to confirm that they correspond to true minima. In addition, frequency calculations allow an estimate of zero-point vibrational energy (ZPVE) corrections. Anharmonic vibrational frequencies and intensities have been obtained in order to aid in a possible experimental detection by IR spectroscopy. In that case an all-electron DZP (double-zeta plus polarization) basis set[24-26] was used for Ag and Au atoms. Electronic energies were subsequently refined carrying out CCSD(T) calculations[27] (coupled cluster with singles and doubles and a perturbative inclusion of triple excitations) with the aug-cc-pVTZ+PP basis set.

The Gaussian 09[28] suite of programs were used generally for MP2 geometries, harmonic frequencies, and CCSD(T) electronic energies, whereas the CFOUR[29] package was employed mainly for anharmonic frequencies and vibration-rotation interaction constants. In order to get deeper insight into the nature of the metal-carbon bond, a topological analysis of the electronic density within the framework of the Quantum Theory of Atoms in Molecules (QTAIM)[30] has been carried

out. The AIMALL package[31] was employed for this analysis.

Table 1. *Ab initio* energies are included for the predicted species Equilibrium rotational constants (MHz), dipole moments (Debye), and relative energies (kcal/mol) for the different MC_3N isomers (M=Cu, Ag, Au). Rotational constants were obtained at the MP2/aug-cc-pVTZ+PP level and dipole moments at the CCSD/aug-cc-pVTZ+PP level on the MP2 geometry. Relative energies were computed at the CCSD(T) level with the same basis set and corrected with ZPE energies at the MP2 level.

Species	B_e	μ	ΔE
$^{63}CuCCCN$	1003.6	8.94	0.0
$^{65}CuCCCN$	992.7		
$^{107}AgCCCN$	787.4	9.37	0.0
$^{109}AgCCCN$	783.5		
$^{197}AuCCCN$	733.3	7.30	0.0
$^{63}CuCCNC$	1056.0	7.94	27.90
$^{65}CuCCNC$	1044.3		
$^{107}AgCCNC$	825.8	8.32	29.99
$^{109}AgCCNC$	821.7		
$^{197}AuCCNC$	768.1	6.09	27.91
$^{63}CuNCCC$	1094.4	13.11	36.12
$^{65}CuNCCC$	1082.7		
$^{107}AgNCCC$	843.72	14.14	37.88
$^{109}AgNCCC$	839.6		
$^{197}AuNCCC$	785.4	11.77	56.92

Results and discussion

Analysis of the rotational spectra. In order to guide the analysis of the rotational spectrum, searches for the plausible minima on the potential energy surfaces of CuC_3N, AgC_3N and AuC_3N have been carried out by *ab initio* methods. In addition to the MCCCN and MNCCC connectivities, which are obvious candidates to be produced from the BrCCCN precursor, MCCNC isomers were also found to be relatively stable. Other linear or cyclic isomers were found to lie higher in energy. Therefore only results for MCCCN, MNCCC, and MCCNC isomers are provided. The equilibrium rotational constants, dipole moments, and relative energies for these isomers, employed to assign the rotational spectra, are presented in Table 1. All reported structures are true minima on the respective potential energy surface. The only exception is AuNCCC, which has an imaginary degenerate vibrational frequency, corresponding to a π bending mode, of 57i cm^{-1}. Following this mode a bent structure is finally reached, lying just 0.4 kcal/mol below linear AuNCCC at the CCSD(T) level, reflecting the rather flat nature of the potential surface in the surroundings of the linear species. Therefore, this bent species lies about 56.5 kcal/mol higher in energy than the lowest-lying AuCCCN species (see Table 1). In order to maintain a

homogeneous discussion of the bonding for all Cu, Ag, and Au cyanoacetylides, the AuNCCC linear structure will be assumed in what follows. Nevertheless, the detailed molecular structure of the bent AuNCCC is reported in the Supplementary Information (Figure S1).

Wide frequency scans from 3.8 to 4.5 GHz were directed to detect spectral signatures corresponding to the $J = 2–1$ rotational transitions of the three plausible isomers of CuC_3N according to the transition frequencies calculated from the estimated rotational constants of Table 1. Two clusters of lines centered around 3980 and 4025 MHz, with a very complex hyperfine structure showing many fully resolved components, were finally observed. The patterns of these clusters appeared to be very similar with an intensity ratio of about 2:1 in accordance with the natural abundances of ^{63}Cu and ^{65}Cu of 69 % and 31 %, respectively. These two clusters of lines were consequently attributed to CuC_3N isotopologues containing ^{63}Cu and ^{65}Cu. The corresponding rotational transitions $J = 3–2$ and $J = 4–3$ were then predicted and observed. The roughly estimated value of the rotational constants for the ^{63}Cu isotopomer of CuC_3N is $B \approx 1006$ in excellent agreement with the predicted value of 1003.6 for the of copper cyanoacetylide CuCCCN isomer, indicating that this species is generated in the supersonic expansion of our experiment. Furthermore, the relative energies shown in Table 1 confirm that CuCCCN is the most stable isomer. Once the generated species in the experiment has been characterized, more precise theoretical predictions of the rotational parameters, including centrifugal distortion, vibration-rotation interaction, and nuclear quadrupole coupling constants were carried out. The results are provided in Table 2 along with experimental values.

Table 2. Experimental and theoretical spectroscopic constants for CuCCCN. Theoretical values have been calculated at the MP2/aug-cc-pVTZ+PP level and the rotational constants corrected including vibration-rotation interactions.

Parameter [a]	$^{63}CuCCCN$		$^{65}CuCCCN$	
	Experimental	Theoretical	Experimental	Theoretical
B	1006.37993(6) [b]	1004.5	995.44479 (7)	993.6
D	0.0331 (25)	0.0308	0.0334 (27)	0.0310
$eQq(Cu)$	21.9185 (15)	21.963	20.2900 (62)	20.364
$eQq(N)$	-4.0861(14)	-3.875	-4.0853 (17)	-3.709
$C_I(Cu)$	2.13 (9)		2.13^{fixed}	
rms	0.9		0.7	
N	36		22	

[a] B is the rotational constant in MHz, D is the is the quartic centrifugal distortion constant in kHz, eQq electric nuclear quadrupole coupling constants in MHz, C_I is the nuclear spin-rotation constant, the rms deviation of the fit is in kHz and N is the number of measured transitions. [b] Standard error in parentheses in units of the last digit.

CuCCCN possesses two nuclei with quadrupole moment, ^{14}N ($I = 1$) and ^{63}Cu or ^{65}Cu ($I = 3/2$). The interaction at the nuclei of these quadrupole moments with the electric field gradient created by the rest of the molecular charges causes the coupling of the nuclear spin moments to the overall rotational momentum. Hence, each rotational transition of CuCCCN carried the nuclear quadrupole hyperfine pattern expected for the presence of either a ^{63}Cu ($I = 3/2$) or a ^{65}Cu ($I = 3/2$) nucleus and the additional quadrupolar effect of the ^{14}N ($I = 1$)

ARTICLE

nucleus giving rise to a very complex hyperfine pattern as shown in Figure 2 for the J = 2–1 rotational transition. Therefore, nuclear quadrupole coupling constants were predicted (see values in Table 2) and used to model the
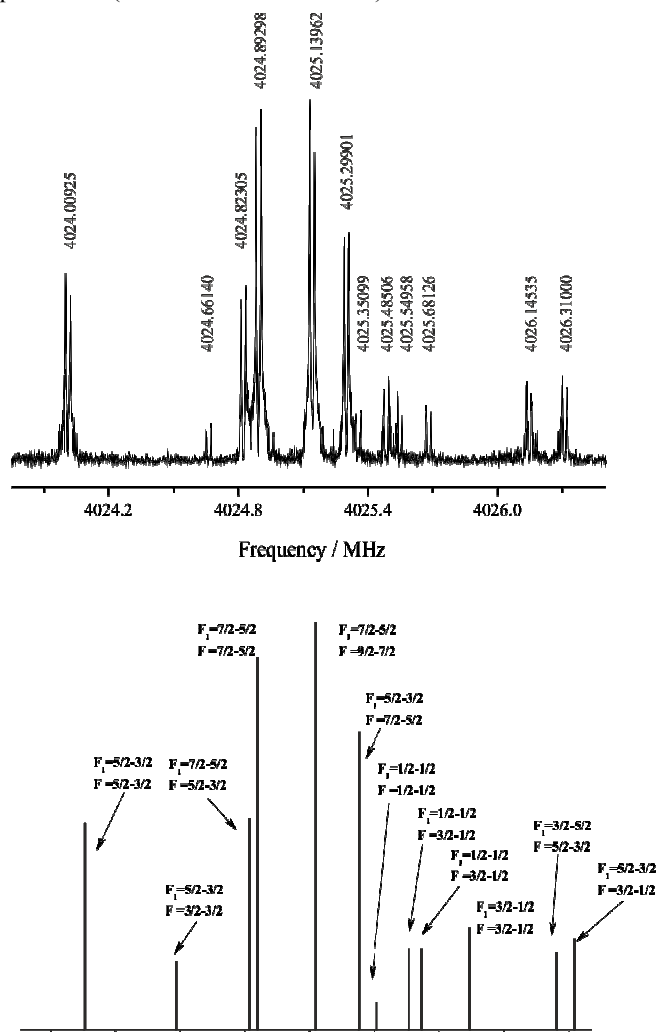

Figure 2. (Upper panel) Central section of the J = 2–1 rotational transition of of ^{63}CuCCCN near 4.0 GHz. The nuclear quadrupole coupling hyperfine structure arising from both from both ^{63}Cu (I=5/2) and ^{14}N (I=1) nuclei is clearly resolved. The coaxial arrangement of the adiabatic expansion and the resonator axis produces an instrumental Doppler doubling. The resonances frequencies are calculated as the average of the two Doppler components. (Lower panel) Theoretical simulation of the nuclear quadrupole hyperfine structure for the J = 2–1 rotational transition of ^{63}CuCCCN isomer.

hyperfine structure. On this basis, all hyperfine components were ascribed as shown in Figure 2. A total of 36 and 22 hyperfine components (Tables S1 and S2 of the Supplementary Material) were measured for ^{63}CuCCCN and ^{65}CuCCCN respectively. The energy levels involved in each transition are labeled with the quantum numbers J, F_1 and F where $F_1 = J + I_{Cu}$ and $F = F_1 + I_N$. The CuCCCN spectra were fit[32] with a standard $^1\Sigma$ Hamiltonian with the form:

$$H = H_R + H_Q(Cu) + H_Q(N) + H_{nsr}$$

where H_R contains rotational and centrifugal distortion

parameters, $H_Q(Cu)$ and $H_Q(N)$ the quadrupole coupling interactions for ^{63}Cu/^{65}Cu and N nuclei respectively while H$_{nsr}$ describes the nuclear spin-rotation terms.

The experimental values for the rotational parameters B_0 and D, the electric quadrupole coupling constants eQq for the ^{63}Cu, ^{65}Cu and ^{14}N nuclei along with the nuclear spin-rotation parameter C_I for the copper nucleus were derived from the analysis are listed in Table 2, along with the theoretical ones. Attempting to fit this last constant for the ^{14}N nucleus resulted in values that were undefined to within their 1σ uncertainties. The standard deviation obtained for the fit are between 0.7 and 0.9 kHz.
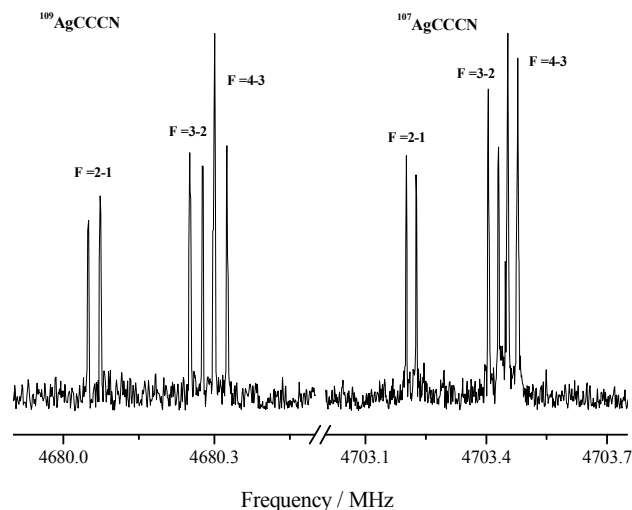

Figure 3. Spectra of the two isotopologues of AgC$_3$N showing the three quadrupole hyperfine components of the J = 2–1 rotational transition near 4.0 GHz due to the ^{14}N (I=1) nucleus.

The expected spectrum for AgC$_3$N should to be simpler than that for CuC$_3$N since only the quadrupole coupling interactions due to the ^{14}N nucleus will contribute to the hyperfine structure. Based on the theoretical calculations, the J = 2–1 rotational transition was searched for AgC$_3$N isomers in the frequency range from 3.0 to 3.4 GHz. Two groups of lines with very similar intensity (Figure 3) were attributed to the ^{107}AgC$_3$N and ^{109}AgC$_3$N isotopologues for which the isotopic ratio (^{107}Ag: ^{109}Ag = 52:48) is consistent with observed intensities. After that, rotational transitions at 4.7, 6.2 and 7.8 corresponding to J = 3–2, J = 4–3 and J = 5–4 were assigned and measured. Approximated values of the rotational constants of 784 and 780 MHz were derived for these species that unequivocally confirm the presence of ^{107}AgCCCN and ^{109}AgCCCN isomers. A total of 11 hyperfine components for each AgCCCN isotopomer were fitted using the following standard $^1\Sigma$ Hamiltonian containing rotation, nuclear quadrupole, and nuclear spin-rotation interactions:

$$H = H_R + H_Q(N) ,$$

to obtain the experimental values of the rotational constants B_0 and D and the electric nuclear quadrupole coupling constant eQq for the ^{14}N nucleus (Table 3).

In the case of AuC$_3$N, frequency scans were conducted to search for the J = 4–3 transition in the frequency interval of 5.7-6.3 GHz. One cluster of lines showing hyperfine structure was detected centered in 5797 MHz (See Figure 4). In addition,

another four rotational transitions at 2.9, 4.3, 7.2 and 8.7 GHz corresponding to $J = 2–1$, $J = 3–2$, $J = 5–4$ and $J = 6–5$ respectively were measured. As in the cases of CuC_3N and AgC_3N the experimental value of the rotational constant for the

Table 3. Experimental and theoretical spectroscopic constants for AgCCCN. Theoretical values have been calculated at the MP2/aug-cc-pVTZ+PP level and the rotational constants corrected including vibration-rotation interactions.

Parameter [a]	[107]AgCCCN		[109]AgCCCN	
	Experimental	Theoretical	Experimental	Theoretical
B	783.90338(64)[b]	787.9	780.04459(75)	784.0
D	0.0258 (16)	0.0242	0.0251 (18)	0.0221
eQq(N)	-4.0767 (93)	-3.703	-4.068 (11)	-3.703
rms	0.6		0.6	
N	11		11	

[a] B is the rotational constant in MHz, D is the is the quartic centrifugal distortion constant in kHz, eQq electric nuclear quadrupole coupling constants in MHz, the rms deviation of the fit is in kHz and N is the number of measured transitions. [b] Standard error in parentheses in units of the last digit.

observed isomer ($B \approx 725$ MHz) clearly points to the observation of the AuCCCN isomer.

AuCCCN as CuCCCN possesses two nuclei with quadrupole moment. With ^{197}Au ($I=3/2$) and ^{14}N ($I = 1$) nuclei, each rotational transition of AuCCCN presents a very complex hyperfine pattern as shown in Figure 4 for the $J = 4–3$ rotational transition. The assignment of each of the hyperfine components becomes more difficult due to the absence of reliable *ab initio* predicted value for the electric nuclear quadrupole coupling constant for the ^{197}Au nucleus. Obtaining reliable quadruple coupling constants for ^{197}Au in gold-containing compounds is not an easy task and in many cases a poor agreement, when compared to the experimental values, is obtained.[33] Even with sophisticated *ab initio* methods incorporating relativistic effects, serious difficulties have been found when trying to
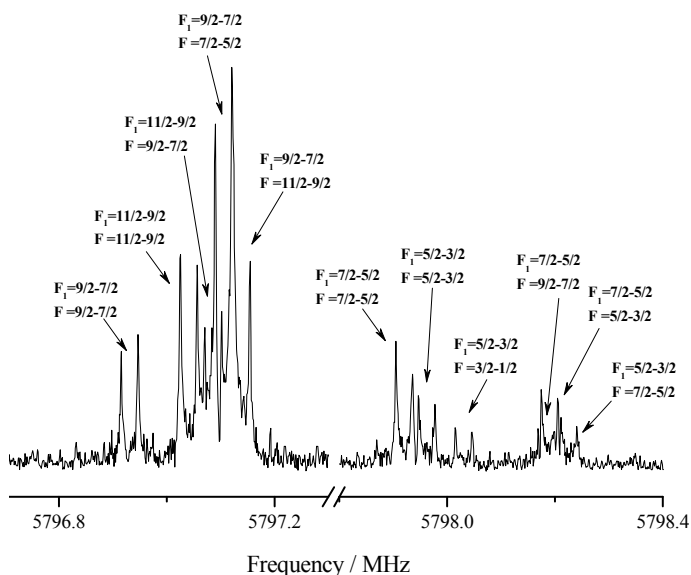
Figure 4. Spectrum of a section of the $J = 4–3$ rotational transition of AuC_3N near 5.8 GHz showing the multiple hyperfine components arising from both ^{197}Au (I=5/2) and ^{14}N (I=1) nuclei.

predict nuclear quadruple coupling constants for ^{197}Au in gold molecules.[34] Due to the lack of reliable theoretical data, an estimation of the eQq for the ^{197}Au nucleus were done taking into consideration previous experimental data for the eQq value of ^{197}Au in related molecular systems.[35] In this manner, up to hyperfine components were fitted using a standard $^1\Sigma$ Hamiltonian with the form:

$$H = H_R + H_Q(Au) + H_Q(N).$$

The fit rendered the rotational parameters B_0 and D and the electric nuclear quadrupole coupling constants for the ^{197}Au and ^{14}N nuclei, which are listed in Table 4. Attempts to fit nuclear spin-rotation parameter C_I for ^{197}Au and ^{14}N nuclei resulted in values that were undefined to within their 3σ uncertainties.

Table 4. Experimental and theoretical spectroscopic constants for AuCCCN. Theoretical values have been calculated at the MP2/aug-cc-pVTZ+PP level and the rotational constants corrected including vibration-rotation interactions.

Parameter [a]	[197]AuCCCN	
	Experimental	Theoretical
B	724.668782 (26)	733.8
D	0.0146 (5)	0.0134
eQq(Au)	36.0960 (30)	-
eQq(N)	-4.1587 (29)	-3.790
rms	0.5	
N	40	

[a] B is the rotational constant in MHz, D is the is the quartic centrifugal distortion constant in kHz, eQq electric nuclear quadrupole coupling constants in MHz, the rms deviation of the fit is in kHz and N is the number of measured transitions. [b] Standard error in parentheses in units of the last digit.

Analysis of the Molecular Structure. A reasonable agreement between experimental and theoretically predicted spectroscopic parameters is generally observed in Tables 2-4. In the case of CuCCCN, the predicted rotational constants are within 2 MHz of the experimental values. This remarkable agreement slightly deteriorates when moving down the group, with a discrepancy of around 9 and 11 MHz for AgCCCN and AuCCCN respectively. It should be noted that the trend in the centrifugal distortion constants is well reproduced by theory. Quadrupole coupling constants are in general consistently predicted (except in the case of ^{197}Au, as explained before), even though they are slightly low for nitrogen, but are in excellent agreement for copper. This agreement suggests that the employed theoretical methods seem appropriate for this kind of systems. In what follows we will try to shed light into the molecular structure and bonding in MC_3N compounds.

Table 5. Equilibrium geometrical parameters for the different MC_3N isomers (M=Cu, Ag, Au) obtained at the MP2/aug-cc-pVTZ+PP level. Distances are given in Ångstroms.

ARTICLE

It can be seen in Table 5 that the different C-C and C-N distances for all MCCCN isomers are quite similar. Furthermore, they are very close to the distances found in HCCCN ($d(C_1\text{-}C_2)$=1.2174 Å; $d(C_2\text{-}C_3)$=1.3721 Å; $d(C_3\text{-}N)$=1.1772 Å) and CCCN ($d(C_1\text{-}C_2)$=1.2195 Å; $d(C_2\text{-}C_3)$=1.3731 Å; $d(C_3\text{-}N)$=1.1766 Å) at the same level of theory. Only the C_1-C_2 distance seems to be slightly lengthened in MCCCN species as a consequence of forming the M-C bond. These geometrical parameters suggest that MCCCN (M=Cu, Ag, Au) can be mainly described by a cyanoacetylene-type valence-bond description:

$$M-C \equiv C-C \equiv N:$$

On the other hand, in MNCCC isomers the C-C distances are considerably altered respect to those found in CCCN. The central C-C distance is shortened whereas the terminal C-C bond is lengthened, taking values much closer to each other. This suggests that a valence-bond structure of the cumulene-type might have a significant role in describing these isomers.

$$M-\ddot{N}=C=C=C:$$

It is interesting to note that the M-C distance in MCCCN isomers is shorter in all cases than the M-N distance in MNCCC ones. This is particularly evident in the CuCCCN/CuNCCC system, with a difference of 0.1 Å. It is worth mentioning that in the system CuCN/CuNC, as well as in AgCN/AgNC and AuCN/AuNC, the behavior is just the opposite, since the M-C distance is longer than the M-N one.[11,12] This behavior suggests a weaker ability for M-N bonding in MNCCC compounds than in the corresponding isocyanides, MNC. This behavior has already been pointed out by Petrie[36], when studying NaC_3N, MgC_3N, and AlC_3N systems. As pointed out by Petrie, the $CCCN^-$ ligand has a greater propensity for the negative charge to be localized upon the terminal carbon atom than the CN^- ligand.[36]

In the case of MCCNC isomers the main valence-bond structure can be written as:

$$M-C \equiv C-\ddot{N}=C:$$

although there is a strong delocalization of the nitrogen electron lone-pair into the vacant p orbital of the terminal carbon atom, approaching a $N \equiv C$ triple bond. The bond distances are again compatible with this valence-bond picture.

Apparently one should expect longer M-C and M-N distances as one goes down the group 11 elements. This trend is observed when comparing the Cu-C and Cu-N distances with the corresponding Ag-C and Ag-N ones. However, the trend is reversed in the case of gold, since Au leads to shorter distances than Ag in both MCCCN and MNCCC isomers. This behavior should be mainly attributed to relativistic effects[11,37] which are particularly strong for gold. A similar trend was found in the electronic charge density (see Table 7 *vide infra*).

From the relative energies collected in Table 1 it can be seen that C-metal bonding is clearly preferred over N-metal bonding for Cu, Ag, and Au. In fact the energy differences between the MCCCN/MNCCC isomers are considerably higher than those found for the MCN/MNC system.[11] The energy differences in MCN/MNC compounds are around 10, 12, and 27 kcal/mol for Cu, Ag, and Au, respectively.[11] These values
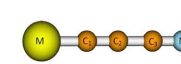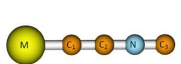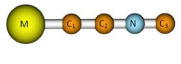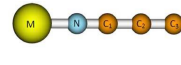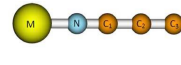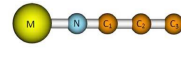
suggest a much more pronounced preference for C-bonding in CCCN than in CN. The dissociation values for the MCCCN isomers (103.2, 90.25, and 98.02 kcal/mol for CuCCCN, AgCCCN, and AuCCCN, respectively) are relatively high, suggesting quite strong M-C bonds for the three metals. The predicted dissociation energies for MCCCN species are even higher than those estimated for MCN compounds.[11] On the other hand, the dissociation energies for MNCCC isomers (67.08, 52.37, and 41.1 kcal/mol for CuNCCC, AgNCCC, and AuNCCC, respectively) are smaller than those predicted for MNC species.[11] The observed trends along the Cu-Ag-Au series are completely similar to those found for the cyanide/isocyanide compounds: for MCCCN isomers the dissociation energies follow the order Cu>Au>Ag, whereas for MNCCC the stability order is Cu>Ag>Au. As suggested by Frenking et al.,[11] the trend in the bond energies is also strongly influenced by relativistic effects.

Table 6. Nuclear quadrupole coupling constant for the Cu nucleus and Cu-C bond distances for some Cu-containing species.

Species	eQq (Cu) /MHz		Cu-C / Å	
	Exp.	Theo.	Exp.	Theo.
CuCN	24.523 (17) [a]	25.441	1.82962 [c]	1.8169
CuCCCN	21.9192 (35) [b]	21.963	-	1.8056
CuCCH	16.391 (21) [a]	16.172	1.8177 [a]	1.8018

[a] Ref. 38; [b] This work; [c] Ref. 1

In order to analyze the properties of the M-C bond, we may compare the electronic quadrupole coupling constant for the Cu nucleus with those found for other copper containing species. The experimental and theoretically estimated eQq(Cu) values for CuCCCN, CuCN, and CuCCH are shown in Table 6, along with the Cu-C experimental and theoretical bond lengths. It is remarkable the good agreement between the theoretical estimations of quadrupole constants and the experimental ones for the three species. As pointed out by Ziurys et al.,[38] it is not always easy to obtain good theoretical values for copper quadrupole constants. From the eQq(Cu) values shown in Table 6, it can be concluded that CuCCCN has a Cu-C bond with an ionic character lying between those of CuCN and CuCCH, the

Species	$d(M\text{-}C_1)$	$d(C_1\text{-}C_2)$	$d(C_2\text{-}C_3)$	$d(C_3\text{-}N)$	
CuCCCN	1.8056	1.2359	1.3691	1.1792	
AgCCCN	1.9927	1.2347	1.3696	1.1791	
AuCCCN	1.8583	1.2277	1.3676	1.1786	
	$d(M\text{-}C_1)$	$d(C_1\text{-}C_2)$	$d(C_2\text{-}N)$	$d(N\text{-}C_3)$	
CuCCNC	1.8056	1.2320	1.3141	1.1895	
AgCCNC	1.9911	1.2309	1.3149	1.1893	
AuCCNC	1.8624	1.2231	1.3110	1.1899	
	$d(M\text{-}N)$	$d(N\text{-}C_1)$	$d(C_1\text{-}C_2)$	$d(C_2\text{-}C_3)$	
CuNCCC	1.9060	1.1892	1.3239	1.2717	
AgNCCC	2.0164	1.1889	1.3270	1.2708	
AuNCCC	1.8884	1.1872	1.3191	1.2734	

latter exhibiting the largest covalent character. This is clearly reflected in the Cu-C bond distances, with decreasing values in

Physical Chemistry Chemical Physics Accepted Manuscript

the order CuCN, CuCCCN, CuCCH.

More insight into the ionic/covalent character of M-C bonding, as well as about the competition between C-metal and N-metal isomers, can be obtained through an analysis of the electronic density within the framework of the Quantum Theory of Atoms in Molecules (QTAIM).[30] This analysis was performed employing the CCSD/aug-cc-pVTZ electronic density for the MCCCN/MNCCC isomers (M=Cu, Ag, Au), as well as for the MCN/MNC compounds for comparison. A detailed account of the significance of the different magnitudes employed in QTAIM can be found in the work of Bader[30,39] and Cremer and Kraka.[40] Just to summarize the main concepts related to our present work, we may point out that in QTAIM two limiting types of interactions can be identified, namely shared and closed-shells interactions. Shared interactions, typical of covalent compounds, are characterized by relatively large values of the electronic density, $\rho(r)$, and negative values of its Laplacian, $\nabla^2\rho(r)$, at the bond critical point. On the other hand, shared interactions, which are usually found in ionic bonds or van der Waals molecules, have relatively low values of $\rho(r)$ and positive values of the Laplacian, $\nabla^2\rho(r)$. In addition, the total energy density $H(r)$ provides some clues about the covalent character of a bond. $H(r)$ is defined as the sum of the potential energy density, $V(r)$, and the gradient kinetic energy density $G(r)$ at a critical point. Negative values of $H(r)$ are typical of covalent interactions, whereas ionic interactions and van der Waals systems are characterized by positive values of $H(r)$. The $|V(r)|/G(r)$ ratio also helps to analyze quantitatively the covalent character of an interaction. In covalent interactions the value of this relationship is greater than 2, whereas it is smaller than 1 for non-covalent interactions and between 1 and 2 for partially covalent bonds.

Table 7. Local topological properties[a] (in a.u.) of the electronic charge density distribution calculated at the position of the bond critical points for the different MCCCN/MNCCC species.

Species	Bond	$\rho(r)$	$\nabla^2\rho(r)$	$\|V(r)\|/G(r)$	$H(r)$	$\delta(A\text{-}B)$
CuCCCN	Cu-C1	0.144	0.386	1.431	-0.073	0.852
	C1-C2	0.402	-1.244	2.844	-0.679	1.927
	C2-C3	0.320	-1.131	4.341	-0.403	1.089
	C3-N	0.463	-0.264	2.083	-0.863	1.836
CuNCCC	Cu-N	0.138	0.641	1.268	-0.059	0.686
	N-C1	0.446	-0.415	2.145	-0.821	1.527
	C1-C2	0.335	-0.912	2.787	-0.517	1.274
	C2-C3	0.387	-1.448	3.392	-0.622	1.706
AgCCCN	Ag-C1	0.126	0.305	1.422	-0.056	0.849
	C1-C2	0.401	-1.229	2.824	-0.680	1.933
	C2-C3	0.320	-1.127	4.333	-0.403	1.087
	C3-N	0.463	-0.264	2.083	-0.864	1.836
AgNCCC	Ag-N	0.110	0.448	1.255	-0.038	0.637
	N-C1	0.446	-0.408	2.142	-0.820	1.546
	C1-C2	0.334	-0.922	2.818	-0.512	1.264
	C2-C3	0.387	-1.439	3.364	-0.624	1.717
AuCCCN	Au-C1	0.194	0.160	1.775	-0.136	1.103
	C1-C2	0.402	-1.230	2.845	-0.672	1.930
	C2-C3	0.321	-1.135	4.387	-0.402	1.081
	C3-N	0.463	-0.243	2.075	-0.864	1.841
AuNCCC	Au-N	0.171	0.523	1.413	-0.091	0.929
	N-C1	0.438	-0.233	2.079	-0.798	1.471
	C1-C2	0.337	-0.874	2.713	-0.525	1.285
	C2-C3	0.387	-1.456	3.434	-0.618	1.691

[a] The electronic charge density $[\rho(r)]$, the Laplacian $[\nabla^2\rho(r)]$, the relationship between the potential energy density $V(r)$ and the lagrangian form of kinetic energy density $G(r)$), the total energy density, $[H(r)]$, and the bond index between atoms A and B $[\delta(A\text{-}B)]$

The main results from the QTAIM analysis are summarized in Table 7. The topological properties of carbon–carbon and carbon-nitrogen bond critical points show the typical characteristics of shared interactions: large values of $\rho(r)$, negative values of its Laplacian, $|V(r)|/G(r)$ ratios greater than 2, and negative values of the total energy density. However as it can be seen from Table 7 the electronic charge density magnitude for MCCCN and MNCCC isomers is clearly different. Thus, for MCCCN arrangements C1-C2 bonds show a greater electronic charge density than C2-C3 bonds in accordance with the acetylene-type valence-bond description of these compounds, whereas in the MNCCC isomers both C1-C2 and C2-C3 bonds have similar electronic charge densities in agreement with a cumulene-type valence-bond description.

More interesting are the characteristics of the M-C and M-N bonds in MCCCN and MNCCC isomers, respectively. In all cases relatively low values of the electron density are encountered, as well as positive values of $\nabla^2\rho(r)$. However, $|V(r)|/G(r)$ ratios are between 1 and 2, and the energy density takes negative values, although small in magnitude. On the other hand metal-carbon bonds show relatively large delocalization indices $\delta(A,B)$ and points toward a relatively important covalent contribution. Therefore, all these M-C and M-N bonds can be classified as closed-shell interactions (mainly ionic in nature) with a small degree of covalence. From these values it can be inferred a slightly more covalent character in M-C bonds than in M-N bonds (lager values of $\rho(r)$, smaller values of its Laplacian, and larger absolute values of $H(r)$). It is also interesting to point out that, based on the same arguments, AgCCCN/AgNCCC species show slightly less covalent character than their copper counterparts. On the other hand, this trend is reversed in the case of gold, because the higher magnitudes suggest that AuCCCN/AuNCCC isomers exhibit a slightly greater covalent character than AgCCCN/AgNCCC species.

Concerning the preference for the MCCCN arrangement over the MNCCC one, the QTAIM analysis provides a similar explanation as that suggested by Frenking et al.[11] for the MCN/MNC systems. As in the case of the cyanide/isocyanide species, MCCCN isomers have lower net charges at carbon than MNCCC isomers at the nitrogen atom. However, the interaction with the metal is more favorable in MCCCN due to the distribution of the electron density. The maps of the Laplacian of the electron density for MCCCN/MNCCC, provided in the Supplementary material (Figure S2), show similar distributions as in the case of MCN/MNC.[11] The terminal carbon atom in CCCN has a larger and more diffuse area of charge concentration than the nitrogen atom. As a

Physical Chemistry Chemical Physics Accepted Manuscript

Physical Chemistry Chemical Physics

Page 8 of 10

ARTICLE

View Article Online

DOI: 10.1039/C6CP04474C

Journal Name

consequence, a more favorable interaction of the CCCN unit with the metal is obtained through the carbon atom rather than through the nitrogen atom.[13] In addition, as can be seen in Table 7, the bond index $\delta(A\text{-}B)$ for the M-C bonds are noticeably larger than those for the M-N bonds, indicating that M-C bonds are stronger than M-N ones.

The present experimental study is focused on the rotational spectra of CuCCCN, AgCCCN, and AuCCCN. Nevertheless, we will also provide predictions for the vibrational spectrum of these species. The estimated vibrational frequencies and IR intensities are collected in Table 8. Harmonic vibrational and IR intensities have been computed at the MP2/aug-cc-pVTZ+PP level. Anharmonic corrections have been estimated at the MP2 level employing an all-electron basis set, namely a DZP (double-zeta plus polarization) basis set.[24-26] The final estimations collected in Table V include the anharmonic corrections. The assignment of the normal modes is in some cases approximate, since for some species there are couplings between two bending modes and between two stretching modes. A clear assignment corresponds to the $M\text{-}C_1$ stretching mode, which has vibrational frequencies for CuCCCN, AgCCCN, and AuCCCN in agreement with the corresponding bonding distances (see Table 1). For the three compounds the predicted IR intensity for this mode is moderate. The most intense lines in the IR spectrum for both AgCCCN and AuCCCN are predicted to correspond to a bending mode and the $C_3\text{-}N$ stretching one. For the CuCCCN compound these two modes are also very intense, but the $C_2\text{-}C_3$ stretching mode has the most intense lines. It is hoped that these predictions could help in an eventual IR experimental study.

Table 8. Anharmonic vibrational frequencies (ω, cm^{-1}) and IR intensities (I, m/mol) for MCCCN (M=Cu,Ag,Au) evaluated at the MP2/aug-cc-pVTZ level.

	Symmetry / Mode	CuCCCN		AgCCCN		AuCCCN	
		ω	I	ω	I	ω	I
1	π MC_1C_2 bend	104	3.78	93	2.59	117	0.09
2	π $C_1C_2C_3$ bend	285	24.80	261	20.59	344	20.82
3	σ $M\text{-}C_1$ stretch	356	9.16	301	12.21	346	2.84
4	π C_2C_3N bend	509	2.26	506	2.93	584	0.28
5	σ $C_2\text{-}C_3$ stretch	965	29.80	947	4.52	1005	6.31
6	σ $C_1\text{-}C_2$ stretch	1992	0.0	1993	0.03	2030	0.47
7	σ $C_3\text{-}N$ stretch	2153	21.78	2157	28.09	2181	46.43

Conclusions

The metallic cyanoacetylides CuCCCN, AgCCCN, and AuCCCN, have been synthesized and characterized in the laboratory using a combination of laser ablation techniques and Fourier transform microwave spectroscopy. A newly constructed ablation-heating source has been proved as an effective method to create metallic cyanoacetylides, using solid samples of BrCCCN as main precursor.

The analysis of the rotational spectra rendered the experimental rotational parameters that are in reasonable good agreement with those predicted theoretically. This investigation has shown that cyanoacetylides of Group 11 elements clearly prefer the MCCCN arrangement. This preference is even more pronounced moving down the group.

An analysis of the bonding has shown that the M-C bonds are mainly ionic in nature with a small degree of covalence. The origin for the preference for the MCCCN arrangement is similar to that found in the MCN compounds[13]. The terminal carbon atom in CCCN has a larger and more diffuse area of charge concentration than the nitrogen atom. The relative energies for the MCCCN/MNCCC compounds suggest a much more pronounced preference for C-bonding in CCCN than in CN. The estimated dissociation energies for MCCCN are even higher than those calculated for MCN compounds, suggesting quite strong M-C bonds for the copper, silver, and gold cyanoacetylides

Notes and references

[a] *Grupo de Espectroscopia Molecular (GEM). Edificio Quifima. Laboratorios de Espectroscopia y Bioespectroscopia. Unidad Asociada CSIC, Parque Científico Uva, Universidad de Valladolid, Paseo de Belén 5, 47011 Valladolid, Spain*

E-mail: jlalonso@qf.uva.es; Phone: +34 983186345

[b] *Departamento de Química Física y Química Inorgánica, Facultad de Ciencias, Universidad de Valladolid, Campus Miguel Delibes, Paseo de Belén 7, 47011 Valladolid, Spain*

E-mail: alargo@qf.uva.es; Phone: +34 983423482

[c] *Institut des Sciences Chimiques de Rennes, École Nationale Supérieure de Chimie de Rennes, CNRS, UMR 6226, 11 Allée de Beaulieu, CS 50837, 35708 Rennes Cedex 7, France*

† Electronic Supplementary Information (ESI) available: [Geometrical parameters the bent structure of AuNCCC, contour maps of the Laplacian distribution of the electron density for the MCCCN and MNCCC isomers and measured frequencies for the nuclear quadrupole coupling hyperfine components of ^{63}CuCCCN, ^{65}CuCCCN, ^{107}AgCCCN, ^{109}AgCCCN and ^{197}AuCCCN.]. See DOI: 10.1039/b000000x/

1. D. B. Grotjahn, M. A. Brewster, L. M. Ziurys, The First Precise Molecular Structure of a Monomeric Transition Metal Cyanide, Copper (I) Cyanide, *J. Am. Chem. Soc.,* **124**, 2002, 5895-5901.

2. M. A. Brewster, L. M. Ziurys, Rotational Spectroscopy of 3d Transition-Metal Cyanides: Millimeter-Wave Studies of ZnCN ($X^2\Sigma^+$), *J. Chem. Phys.,* **117**, 2002, 4853-4860.

3. P. M. Sheridan, L. M. Ziurys, Further Studies of 3d Transition Metal Cyanides: The Pure Rotational Spectrum of NiCN ($X^2\Delta_i$), *J. Chem. Phys.,* **118**, 2003, 6370-6379.

4. P. M. Sheridan, M. A. Flory, L. M. Ziurys, Characterizing the Later 3d Cyanides: The Sub-Millimeter Spectrum of CoCN ($X^3\Phi_i$), *J. Chem. Phys.,* **121**, 2004, 8360-8368.

5. M. A. Flory, R. W. Field, L. M. Ziurys, The Pure Rotational Spectrum of CrCN ($X^6\Sigma^+$): an Unexpected Geometry and Unusual Spin Interactions *Mol. Phys.,* **105**, 2007, 585-597.

6. C. T. Kingston, A. J. Merer, T. D. Varberg, The Electronic Spectrum of NiCN in the Visible Region, *J. Mol. Spectrosc.,* **215**, 2002, 106-127.

7. J. Lie, P. J. Dagdigian, Observation of the FeNC Molecule by Laser Fluorescence Excitation Spectroscopy. *J. Chem. Phys.,* **114**, 2001, 2137-2143.

8. M. A. Flory, L. M. Ziurys, Millimeter-Wave Rotational Spectroscopy of FeCN ($X^4\Delta_i$) and FeNC ($X^6\Delta_i$): Determining the Lowest Energy Isomer, *J. Chem. Phys.,* **135**, 2011, 184303-184311.

9. L. N. Zack, J. Min, B. J. Harris, M. A. Flory, L. M. Ziurys, Fourier Transform Microwave Spectroscopy of FeCN ($X^4\Delta_i$): Confirmation of the Quartet Electronic Ground State, *Chem. Phys. Lett.,* **514**, 2011, 202-206.

10. A. I. Boldyrev, X. Li, L. S. Wang, Vibrationally Resolved Photoelectron Spectra of CuCN$^-$ and AgCN$^-$ *Ab Initio* Studies of the Structure and Bonding in CuCN, *J. Chem. Phys.,* **112**, 2000, 3627-3632.

11. O. Dietz, V. M. Rayón, G. Frenking, Molecular Structures, Bond Energies, and Bonding Analysis of Group 11 Cyanides TM(CN) and Isocyanides TM(NC) (TM) Cu, Ag, Au), *Inorg. Chem.,* **42**, 2003, 4977-4984.

12. V. M. Rayón, P. Redondo, H. Valdés, C. Barrientos, A. Largo, Cyanides and Isocyanides of First-Row Transition Metals: Molecular Structure, Bonding and Isomerization Barriers, *J. Phys. Chem. A,* **111**, 2007, 6334-6344.

13. N. J. DeYonker, What a Difference a Decade Has Not Made: The Murky Electronic Structure of Iron Monocyanide (FeCN) and Iron Monoisocyanide (FeNC), *J. Phys. Chem. A,* **119**, 2015, 215-223.

14. H. Umeki, M. Nakajima, Y. Endo, Laboratory Detections of SiC$_2$N and SiC$_3$N by Fourier Transform Microwave Spectroscopy, *J. Chem. Phys.,* **141**, 2014, 184303-184306.

15. C. Cabezas, C. Barrientos, A. Largo, J.-C. Guillemin, J. Cernicharo, I. Peña, J. L. Alonso, Generation and Structural Characterization of Aluminum Cyanoacetylide, *J. Chem. Phys.,* **141**, 2014, 104305-104307.

16. J. L. Alonso, C. Pérez, M. E. Sanz, J. C. Lopéz, S. Blanco, Seven Conformers of L-Threonine in the Gas Phase: a LA-MB-FTMW Study, *Phys. Chem. Chem. Phys.* 2009, **11**, 617-627.

17. C. Cabezas, S. Mata, A. M. Daly, A. Martín, J. L. Alonso, J. Cernicharo, LA-MB-FTMW Spectroscopy of AlCCH and AgCCH with a Discharge Source, *J. Mol. Spectrosc.* **278**, 2012, 31-34.

18. C. Cabezas, J. Cernicharo, J. L. Alonso, M. Agúndez, S. Mata, M. Guélin, I. Peña, Laboratory and Astronomical Discovery of Hydromagnesium Isocyanide, *Astrophys. J.,* **775**, 2013, 133-136.

19. C. Bermúdez, S. Mata, C. Cabezas, J. L. Alonso, Tautomerism in Neutral Histidine, *Angew. Chem. Int. Ed.* 2014, **53**, 11015-11018.

20. T. H. Dunning, Gaussian Basis Sets for Use in Correlated Molecular Calculations. I. The Atoms Boron Through Neon and Hydrogen, *J. Chem. Phys.,* **90**, 1989, 1007-1023.

21. N. B. Balabanov, K. A. Peterson, Systematically Convergent Basis Sets for Transition Metals. I. All-Electron Correlation Consistent Basis Sets for the 3d elements Sc–Zn, *J. Chem. Phys.,* **123**, 2005, 064107-064115.

22. D. Figgen, G. Rauhut, M. Dolg, E. Stoll, Energy-Consistent Pseudopotentials for Group 11 and 12 Atoms: Adjustment to Multi-Configuration Dirac–Hartree–Fock, Data *Chem. Phys.,* **311,** 2005, 227-244.

23. K. A. Peterson, C. Puzzarini, Systematically Convergent Basis Sets for Transition Metals. II. Pseudopotential-Based Correlation Consistent Basis Sets for the Group 11 (Cu, Ag, Au) and 12 (Zn, Cd, Hg), Elements *Theor. Chem. Acc.,* **114**, 2005, 283-296.

24. G. G. Camiletti, S. F. Machado, F. E. Jorge, Gaussian Basis Set of Double Zeta Quality for Atoms K through Kr: Application in DFT Calculations of Molecular Properties, *J. Comp. Chem.,* **29**, 2008, 2434-2444.

25. C. L. Barros, P. J. P. de Oliveira, F. E. Jorge, A. Canal Neto, M. Campos, Gaussian Basis Set of Double Zeta Quality for Atoms Rb through Xe: Application in Non-Relativistic and Relativistic Calculations of Atomic and Molecular Properties, *Mol. Phys.,* **108**, 2010, 1965-1972.

26. A. Canal Neto, F. E. Jorge, All-Electron Double Zeta Basis Sets for the Most Fifth-Row Atoms: Application in DFT Spectroscopic Constant Calculations, *Chem. Phys. Lett.*, **582**, 2013, 158-162.

27. K. Raghavachari, G. W. Trucks, J. A. Pople, M. A Head-Gordon, Fifth-Order Perturbation Comparison of Electron Correlation Theories, *Chem. Phys. Lett.,* **157,** 1989, 479-483.

28. G.W.T. M. J. Frisch, H. B. Schlegel, G. E. Scuseria, M. A. Robb, J. R. Cheeseman, G. Scalmani, V. Barone, B. Mennucci, G. A. Petersson, H. Nakatsuji, M. Caricato, X. Li, H. P. Hratchian, A. F. Izmaylov, J. Bloino, G. Zheng, J. L. Sonnenberg, M. Hada, M. Ehara, K. Toyota, R. Fukuda, J. Hasegawa, M. Ishida, T. Nakajima, Y. Honda, O. Kitao, H. Nakai, T. Vreven, J. A. Montgomery, Jr., J. E. Peralta, F. Ogliaro, M. Bearpark, J. J. Heyd, E. Brothers, K. N. Kudin, V. N. Staroverov, T. Keith, R. Kobayashi, J. Normand, K. Raghavachari, A. Rendell, J. C. Burant, S. S. Iyengar, J. Tomasi, M. Cossi, N. Rega, J. M. Millam, M. Klene, J. E. Knox, J. B. Cross, V. Bakken, C. Adamo, J. Jaramillo, R. Gomperts, R. E. Stratmann, O. Yazyev, A. J. Austin, R. Cammi, C. Pomelli, J. W. Ochterski, R. L. Martin, K. Morokuma, V. G. Zakrzewski, G. A. Voth, P. Salvador, J. J. Dannenberg, S. Dapprich, A. D. Daniels, O. Farkas, J. B. Foresman, J. V. Ortiz, J. Cioslowski, D. J. Fox, Gaussian 09, Revision B.01, in, Gaussian, Inc., Wallingford CT, 2010.

29. J. F. Stanton, J. Gauss, M. E. Harding, P. G. Szalay, *CFOUR*, a quantum chemical program package, **2013**.

30. R. W. F. Bader, *Atoms in Molecules: A Quantum Theory*; Clarendon Press: New York, **1990**.

31. T. A. Keith, *AIMAll*, version 13.11.04, Professional, TK Gristmill Software: Overland Park, KS, 2013; http://aim.tkgristmill.com.

32. H. M. Pickett, The Fitting and Prediction of Vibration-Rotation Spectra with Spin Interactions. *J. Mol. Spectrosc.,* **148**, 1991, 371-377.

33. O. K. Poleschuck, V. Branchadell, R. A. Ritter, A. V. Fateev, Quadrupole Coupling Constants and Isomeric Mössbauer Shifts for Halogen-Containing Gold, Platinum, Niobium, Tantalum and Antimony Compounds, *Hyperfine Interact.,* **181**, 2008, 547- 556.

34. M. Pernpointer, P. Schwerdtfeger, B. A. Hess, *Int. J. Quantum Chem.*, **76**, 2000, 371.

35. T. Okabayashi, H. Kubota, M. Araki, N. Kuze, Microwave Spectroscopy ff AgCCH and AuCCH in the $\tilde{X}^1\Sigma^+$ States, *Chem. Phys. Lett.,* **577**, 2013, 11-15.

ARTICLE

Journal Name

36. S. Petrie, Metal-Containing Molecules: Some New Candidates for Interstellar Detection, *Mon. Not. R. Astron. Soc.,* **302**, 1999, 482-490.

37. P. Pyykkö, Relativistic effects in structural chemistry. *Chem. Rev.,* **88**, 1988, 563-594.

38. M. Sun, D. T. Halfen, J. Min, B. Harris, D. J. Clouthier, L. M. Ziurys, The Rotational Spectrum of CuCCH ($X^1\Sigma^+$): A Fourier Transform Microwave DALAS and Millimeter/Sub-Millimeter Study, *J. Chem. Phys.,* **133**, 2010, 174301-174308.

39. R. W. F. Bader, A Quantum Theory of Molecular Structure and its Applications. *Chem. Rev.,* **91,** 1991, 893-928.

40. D. Cremer, E. Kraka, Chemical Bonds without Bonding Electron Density - Does the Difference Electron-Density Analysis Suffice for a Description of the Chemical Bond?, *Angew. Chem. Int. Ed.,* **23**, 1984, 627-628.